Theoretical Predictions of the Start-Up Phase in GMA Welding

Better methods of controlling the start-up phase will improve weld quality

BY P. ZHU, M. RADOS and S. W. SIMPSON

ABSTRACT. A computer simulation of GMAW start-up has been developed that accounts for the voltage-current characteristics of the welding arc, the welding power supply, and the interaction between the moving anode wire and the welding arc. The overall simulation combines models of free-burning arcs and the thermal properties of the moving wire anode. The time-dependent model solves a set of differential equations describing the welding process. Calculations have been made to predict behavior during the gas metal arc welding start-up phase and results compared with experimental observations of voltage, current and arc length. The model successfully predicts the important features of the experimental data, such as the initial arcing phase in which the arc length is much greater than its final value and the welding current is low.

Introduction

GMA welding is one of the most important industrial processes. Due to the complex nature of the process, which involves materials in all four states: the solid, liquid, gas, and plasma phases, many features of this process are yet to be clarified. In order to understand GMA welding, both theoretical development with predictive models and experimental measurements are required. In this work, we develop a time-dependent model and use it to make predictions of welding start-up. The start-up process is an important one, since a section of poor quality weld is often laid down during start-up. Also, from the point of view of developing a useful predictive capability for GMA welding, comparison with experimental parameters during welding start-up provides a valuable check of the accuracy of predictions.

PEIYUAN ZHU, M. RADOS and S. W. SIMPSON are with the Department of Electrical Engineering, University of Sydney, Australia.

The physics of arc welding has been reviewed comprehensively by Lancaster (Refs. 1, 2). Waszink, *et al.*, investigated heat flow in the anode wire, concluding that the melting rate was governed by both ohmic heating and heat flow from the anode surface (Refs. 3, 4). Based on an analysis of previous published results, Waszink and Piena (Ref. 5) derived an approximate expression for heat transfer from the plasma to the anode. Several authors have noted the significant effect of the shielding gas on metal transfer (Refs. 6–8), and, recently, detailed models of molten droplet formation at the anode have been developed (Refs. 9, 10).

The theoretical model of welding start-up described here combines treatments of the welding arc, anode wire, and welding power supply in an overall simulation of the welding system. Previously, the model was applied successfully to predict steady-state characteristics (Ref. 11) in GMA welding under various conditions. The theory described here is an enhancement of our previous model to handle transient processes. To treat these time-varying situations, the one-dimensional description of the liquid drop on the end of the anode wire has been refined.

The main features of the model are described in the following section, while the Comparison of Model Predictions with Experiment section covers the experimental arrangement, including the laser shadowgraph used to make estimates of the arc length optically, and presents model predictions, comparing them with experimental measurements made during welding start-up; measured quantities such as voltage and current and predictions of anode temperature profiles are given.

KEY WORDS

Gas Metal Arc Welding
Arc Start-Up Phase
Time-Dependent Model
Welding Arc
Anode Wire

Dynamic Model of the GMAW Process

We consider a basic welding arrangement (Fig. 1) in which the anode is a moving steel wire and the cathode is a hot-rolled mild steel plate. The spacing between the contact nozzle and the cathode plate is fixed at 20 mm for all the measurements reported here, and the arc is burning in an argon-based shielding gas with 3% oxygen and 5% carbon dioxide. Any possible influence of the motion of the cathode workpiece and the molten welding pool on the welding arc is not included in the model; the combined electrode sheath voltage (anode and cathode) is assumed to have a constant value of 15 V (Ref. 11). Agreement between the model's steady-state predictions and experimental data suggests these approximations are reasonable ones (Ref. 11). It should be noted that, for a short period of time immediately after the arc strikes, the arc will not be in equilibrium and the use of a steady-state arc model with a constant sheath voltage will not hold. However, other time constants associated with the welding process (the anode wire heating time, for example) are orders of magnitude longer, and these dominate behavior during start-up.

The moving anode wire is assumed to exchange energy with the arc plasma and the electrical contact tube at the ends of the wire only. It is modeled using a one-dimensional treatment that assumes a

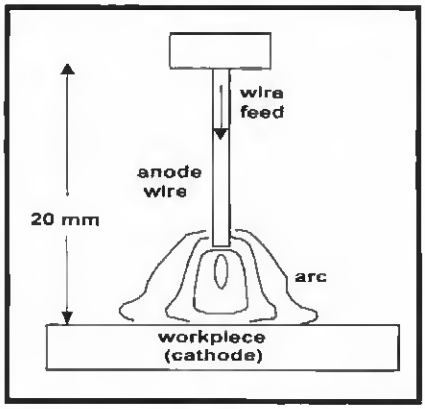

Fig. 1 — Sketch of a conventional GMAW system.

heating source from the arc plasma on the anode tip and accounts for thermal conduction loss along the wire to the contact tube. The wire feed nozzle and contact tube are assumed to have a constant temperature of 300 K (room temperature). The physical processes allowed for in the anode are 1) heat conduction, 2) convection due to the motion of the anode wire, and 3) ohmic heating, with anode blackbody radiation loss neglected.

For heating from the arc plasma, the total power input P to the anode can be written as the sum of three contributions (Ref. 11):

$$P = \frac{A\kappa_{eff}(T_p - T_a)}{l_p} + I\phi_w + I\frac{5K_bT_e}{2e} \quad (1)$$

Here T_p is the arc temperature, which is assumed to have a constant value of 10^4 K at a distance l_p = 0.1 mm away from the anode; T_a is the anode tip temperature; κ_{eff} is the effective thermal conductivity at the anode-plasma interface; A is the arc attachment area; I is the current; ϕ_w is the work function of the anode material; K_b is Boltzmann's constant; and T_e is the electron temperature, which is also assumed to have a value of 10^4 K. The first term on the right side of Equation 1 is a small contribution due to thermal conduction from the plasma to the anode; the second term refers to electron heating associated with the work function of the anode material; the last term accounts for thermal energy carried by the electrons into the anode. The first heating term, related to thermal conduction, is calculated assuming that the current enters the anode over a wire length of 1.5 mm at the tip. This rather arbitrary assumption could be removed by considering the plasma-metal interface in more detail.

The model numerically solves the unedimensional energy conservation equation describing heat flow along the solid anode wire, which can be written as

$$\rho\frac{\partial h}{\partial t} + \rho v_o\frac{\partial h}{\partial z} = \frac{\partial}{\partial z}\left(\kappa\frac{\partial T}{\partial z}\right) + jE + F \quad (2)$$

where ρ is the density of the anode wire, h is the specific enthalpy, v_o is the wire feed speed, E is the electric field along the wire, j is the current density, κ is the thermal conductivity, and F accounts for the heat input from the plasma given in Equation 1. F is assumed to vary linearly from its maximum at the end of the wire to zero over a length of 1.5 mm, corresponding to the arc attachment length on the wire. F is normalized according to $\pi r^2_{wire}\int F dz = P$, where r_{wire} is the anode wire radius. The anode receives energy from the arc plasma near the tip, and, at the other end of the anode, energy flows to the contact tube. The movement of the anode associated with the wire feed was modeled by continually adding grid points onto the wire at the contact tube.

The temperature profile along the anode wire at each time is found from the solution of the energy conservation Equation 2 at each time step, and this can be used to estimate the molten length at the wire tip as a function of time. Metal transfer is a discrete process in which droplets of varying sizes leave the anode. This was handled by discarding 80% of the "molten" elements at the anode tip once a certain critical molten length l_{tip} was reached. The equivalent diameter for spherical droplets D_{drop}, allowing for the 20% of molten metal assumed to remain at the anode, is then given by

$$D_{drop} = 2\left(\frac{3r^2_{wire}l_{tip}}{5}\right)^{1/3} \quad (3)$$

Adjusting l_{tip} allows us to make a simple allowance for the experimentally observed variation of droplet size with welding current (Ref. 12). The relationship used in this study is $l_{tip} \propto 1/I$, with the constant of proportionality between the droplet size and the welding current I adjusted to agree with measured droplet sizes in the spray transfer regime (Ref. 12). The assumed droplet diameter D_{drop} is plotted together with experimental observations (Ref. 12) in Fig. 2. This simple treatment of metal transfer defines the new location of the arc-anode interface before and after each metal transfer, and dynamically calculates the electrode extension and arc length.

If the calculated arc length reaches zero at a certain time, short-circuiting occurs. To allow for the short circuit, the model sets both the sheath voltage and the heating term F in Equation 2 to zero when the anode wire touches the welding plate.

To calculate the change in the arc current I at each time step, Kirchhoff's Voltage Law is solved:

$$L\frac{dI}{dt} = V_{supply} - V_s - V_a - V_i - I(R_c + R_w) \quad (4)$$

where V_{supply} is the voltage supplied to the welding-arc system, V_s is the combined electrode-sheath voltage drop which, based on experimental data in Ref. 13, is assumed to have a constant value of 15 V, V_a is the arc voltage, and V_i is the voltage drop due to the power supply internal resistance. The last term on the right side of the equation accounts for the anode wire, which has resistance R_w, and the nozzle-to-wire contacting resistance R_c. L is the power supply inductance.

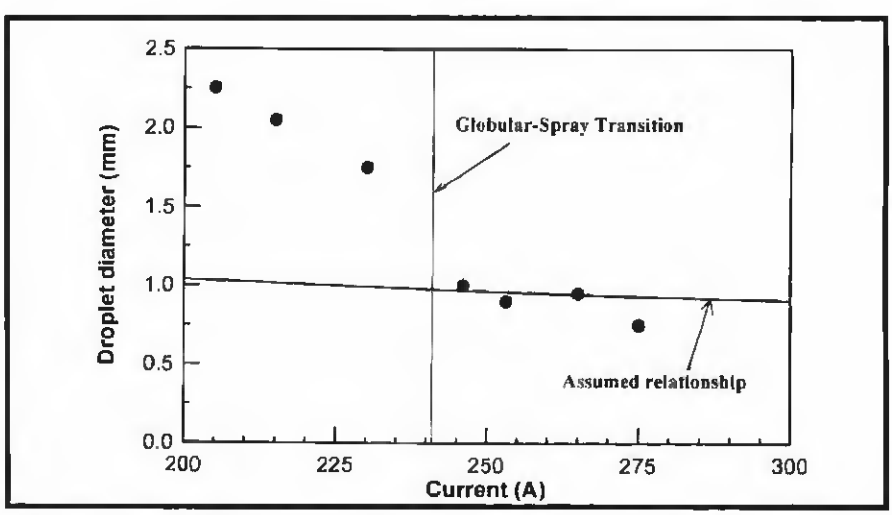

Fig. 2 — Assumed droplet size-current relationship (solid line as indicated) compared with experimental observations from reference (Ref. 12).

The voltage drop due to power supply internal resistance can be represented approximately by a piecewise linear relationship:

$$V_i = R_1 I_0 + R_2(I - I_0), \quad \text{if } I > I_0;$$
$$V_i = R_1 I, \quad \text{if } I \le I_0. \quad (5)$$

From the manufacturer's V-I characteristics for the power supply used in our experimental observations, we have chosen $R_1 = 0.0346\Omega$, $R_2 = 0.0192\Omega$ and $I_0 = 80$ A. The nozzle contact resistance R_c and the power supply inductance L used in the calculation are set to 0.01Ω and 100 μH, respectively. It should be mentioned that, at the large currents present during start-up, the power supply characteristics have a significant effect on behavior.

In Equation 4, R_w and V_a are updated at each time step. R_w is a function of the anode wire temperature profile and the electrode extension. This information comes from the solution to the energy conservation equation for the anode wire described previously (Equation 2). The calculation of the arc voltage V_a necessitates a model for the welding arc. We calculate V_a for each time step using the two-dimensional free-burning arc model of Lowke, *et al.* (Ref. 14), which solves a group of equations including the mass conservation equation, the axial and radial momentum conservation equations, and the energy conservation equation. In this model, the welding arc burning between the two electrodes is assumed to be in local thermodynamic equilibrium and the flow is assumed to be laminar.

In practice, instead of calculating the arc voltage at each time step from the predicted arc length and current, we precalculate the arc voltage-current characteristic as a function of the arc length and tabulate the results to form a reference table to be used by the moving anode model. Using steady-state arc values in this way is equivalent to the assumption that time constants for arc processes are shorter than time constants associated with the rest of the model.

The time-dependent simulation utilizes a simple explicit finite difference method to solve Equations 2 and 4 with the arc voltage for a given arc current and length interpolated from the reference table.

Comparison of Model Predictions with Experiment

Calculations have been compared with experimental data for bead-on-plate welds with a consumable steel anode. The nozzle-to-plate distance for all the results discussed in this paper was 20 mm, and an argon-based shielding gas with 3% oxygen and 5% carbon dioxide was employed. The welding arc transport properties were calculated assuming 2% iron vapor present in the gas to allow for evaporation from electrodes and metal drops in the arc.

Our experimental measurements were carried out using a GMAW system as shown in Fig. 1. The welding voltage was measured at the welding power supply, while the welding current was measured using a Hall effect probe. Both the welding voltage and current were measured with a sampling time of 0.5 ms, which was fast enough to capture the main features of welding start-up.

A laser shadowgraph arrangement (Ref. 15) similar to that described in Ref. 16 was used to make approximate observations of arc lengths during the start-up phase. With the use of a beam expander, a 20 mW He-Ne laser produced a beam that evenly illuminated the welding arc and electrodes. After passing through an interference filter to reduce arc light and an enlarging lens system, the beam impinged on a ground glass screen and the image was recorded by a video camera. Observations were made at intervals of 20 ms, limited by the sampling rate of the video camera used. This sampling rate was too slow to observe the process of single droplet transfer, but was high enough to obtain an overall picture of the changing arc length during weld start-up. The exposure time for each frame was 1/8000 s. Frames that did not clearly show whether a droplet was detached or not were not analyzed, since the distance from the anode surface to the workpiece was uncertain.

Predicted steady-state arc current is plotted against the wire feed rate in Fig. 3 together with experimental data points. Theory and experiment are shown for anode wire diameters of 1.2 and 0.9 mm with a power supply terminal voltage of 30 V. The agreement between steady-state theoretical predictions and experiment is good for both wires.

Figures 4, 5 and 6 show the predicted transient behavior of arc current, power supply terminal voltage, and arc length, respectively, as a function of time during welding start-up and make a comparison with experimental data. The wire feed rate was 11 cm/s, the steel anode diameter was 1.2 mm, and the power supply open circuit voltage was 36.5 V with 5% ripple for these figures. (This value corresponds to the steady-state condition at the same wire feed rate and diameter in Fig. 3.) The experimental voltage measured at the terminals of the welding power supply includes the arc voltage, the voltage drop along the anode wire, and the effect of the contact resistance. The predicted voltages were estimated in the same way.

Figure 7 shows two shadowgraph images reproduced from the video frames. The long arc on the left is an image recorded at time 80 ms, while the shorter arc on the right is an image recorded at time 200 ms.

The sequence of events in Figs. 4–6 is as follows:

1) The cold anode wire feeds down to the cathode surface at the wire feed rate.

2) At time zero, the anode wire contacts the cathode and the current rises

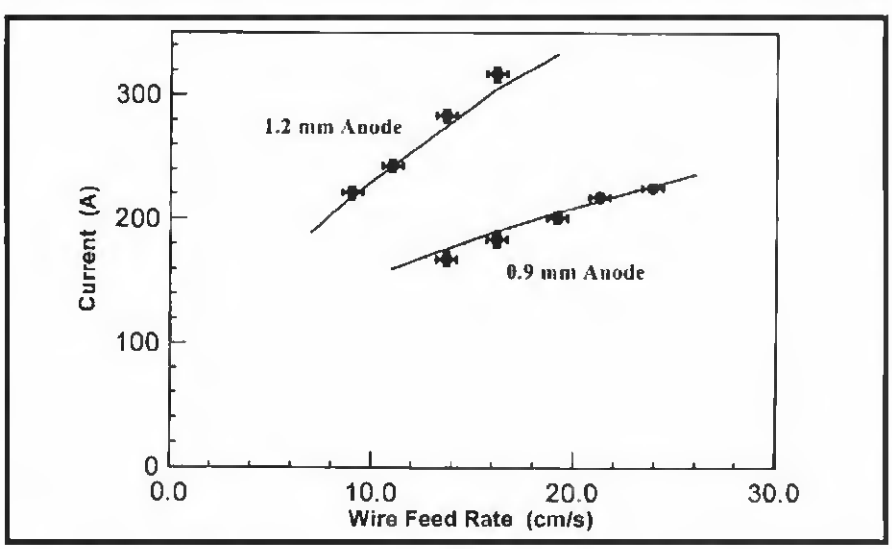

Fig. 3 — Predicted steady-state current as a function of the wire-feed rate for steel wires with diameters of 1.2 and 0.9 mm (solid lines). The experimentally measured data (points) are also shown. The power supply terminal voltage used in both the theoretical calculation and experiment was 30 V.

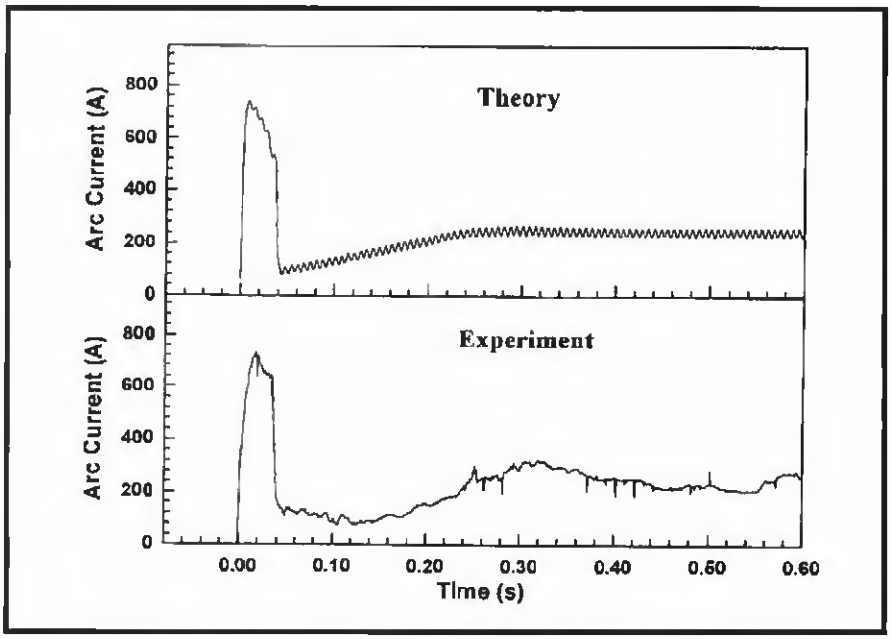

Fig. 4 — Predicted arc current during welding start-up compared with experimental results. Curve A plots the predicted current as a function of time while Curve B shows the experimental results. The wire feed rate used was 11 cm/s, the wire diameter was 1.2 mm, and the open circuit supply voltage was 36.5 V.

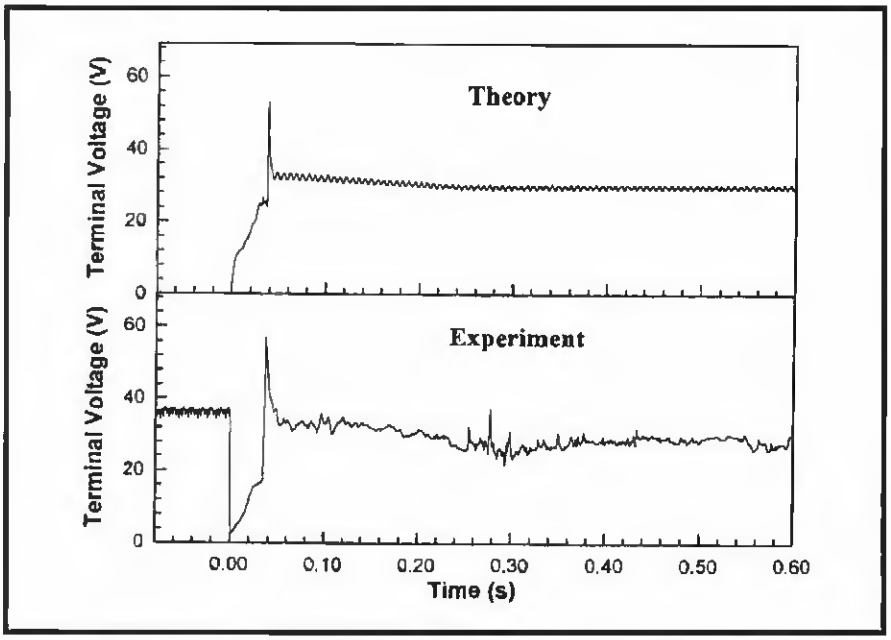

Fig. 5 — Predicted power supply terminal voltage during welding start-up compared with experimental results. Curve A plots the predictions while Curve B shows the experimental results. Experimental parameters were the same as in Fig. 4.

quickly, limited by the circuit inductance. At this time, the theoretical calculation begins.

3) Between time zero and about time 40 ms, the anode wire is short-circuited to the cathode and a large current flows, heating the wire until melting occurs. The predicted "arc length" falls to a negative value of 4.6 mm during this phase due to the continuing wire feed. This should be interpreted as bending of the wire in the arc length, such that the wire length is 24.6 mm in the 20 mm arc length. This bending phenomenon has been observed in the experimental laser shadowgraph images.

4) When the wire melts at around time 40 ms, a long arc is formed (Fig. 6). A large volume of the anode wire is transferred at this point, and frequently intact sections of wire are observed leaving the arc region in the shadowgraph images. At this point, the voltage provided by the power supply can only maintain a low current arc over the large arc length (Fig. 5), which is not sufficient to melt the amount of material being fed down. The arc length then decreases at around the wire feed rate, resulting in an increasing current.

5) There is a slight overshoot in arc current at about 0.3 s, accompanied by a reduced arc length (Fig. 6). In fact, the oscillation is more pronounced in the experimental data than in the predictions, with quite short arc lengths visible. Consider, however, that the estimation of arc length from the shadowgraph images is a relatively crude one in the presence of continuous metal droplet transfer across the arc length.

6) On a longer time scale, the system approaches the steady state.

Several other features in Figs. 4–6 are worth commenting on. The small oscillations in the predicted arc length curves (Fig. 6) show the frequency and the influence of the metal transfer, while the oscillations in both current and voltage traces show the effect of power supply ripple (Figs. 4 and 5).

In Fig. 4, it is observed that the predicted current trace shows a smooth increase from its minimum value, while experimentally the current remains at a low level for longer time. This is partly due to the limitation of our one-dimensional treatment, which cannot properly handle the growth of large droplets at low current. As mentioned in the previous section, we have assumed a larger droplet size for low currents (Fig. 2) to offset some of the error. Overall, the predictions agree reasonably well with the experimental measurements, confirming the predictive capability of the model.

The predicted anode temperature distributions for four different instants in time are plotted in Figs. 8 and 9. It is clear that there are qualitative differences in anode temperature distribution at different stages of the start-up phase. Figure 8A plots the anode temperature distribution at t = 7.27 ms shortly after the anode wire has contacted the cathode surface. It shows an evenly distributed temperature over a length of about 20 mm, which was the electrode extension when short-circuiting started, and the current started to flow. This is a result of ohmic heating due to the high short-circuit current (Fig. 4), which is evenly applied to the initial anode length of 20 mm over the whole short-circuiting period. The temperature gradually

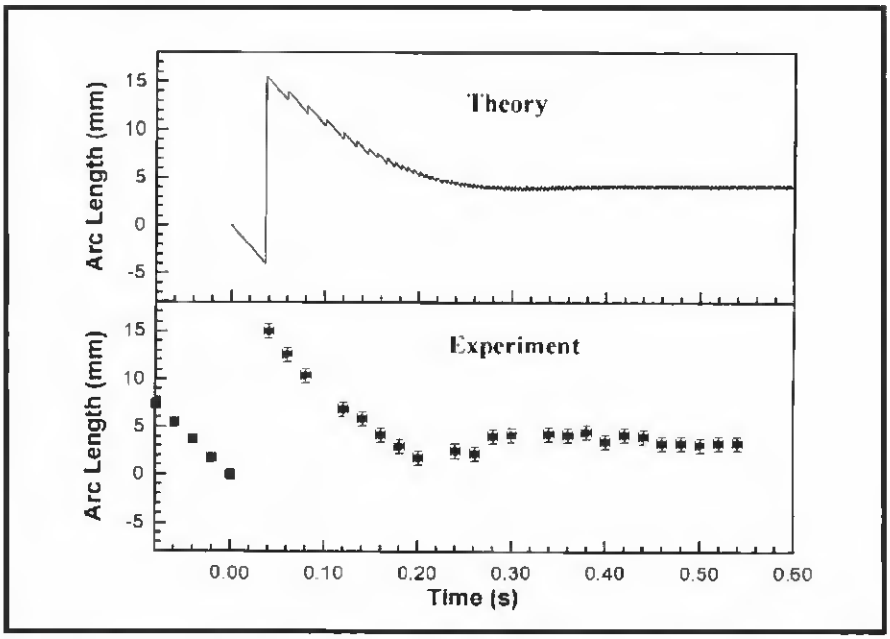

Fig. 6 — Predicted arc length during welding start-up compared with experimental results taken from laser shadowgraph images. Curve A plots the predictions while Curve B shows the experimental results. Experimental parameters were the same as in Fig. 4.

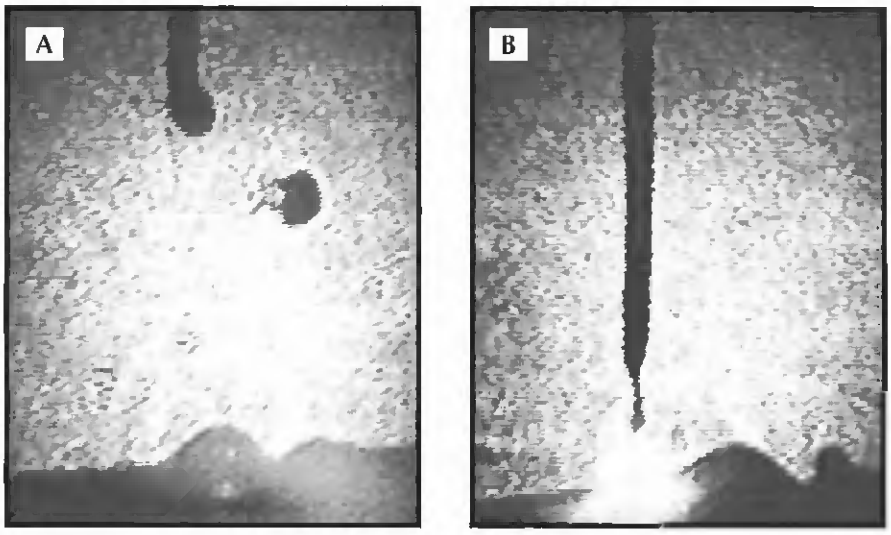

Fig. 7 — Shadowgraph images recorded at times 80 ms (left) and 200 ms (right) during arc start-up.

decreases to the ambient temperature of 300 K at the nozzle end. This temperature gradient can largely be explained by the fact that the anode is fed down and only the initial 20 mm length has been through the whole heating history.

Figure 8B shows the temperature profile at $t = 41.8$ ms, just before the welding arc starts. Again the temperature is uniform over approximately 20 mm, the initial length, and there is a strong temperature gradient near the nozzle where the wire is feeding out. It should be pointed out that the present treatment does not consider any possible heat conduction to the cathode or local contact heating at the end of the anode wire during this short-circuit phase. According to the model, since the length of about 20 mm on the tip side has an even temperature distribution, the entire length will undergo a solid-to-liquid phase change at nearly the same instant when the melting point of 1805 K is reached. In practice, in the presence of the bending stress, it has been observed that entire sections of wire are occasionally detached. Also, in practice, it is observed that often the arc does not strike the first time, and the wire feeds down again, a second section of wire is detached and the arc strikes.

Figure 9A plots the anode temperature profile at $t = 54.6$ ms, shortly after the arc has appeared. It can be seen that heating from the arc has raised the temperature of the anode-arc attachment area (about 1.5 mm in length). This is a result of the dense heating source from the welding arc to the anode wire, which is applied at the attachment area. Since the current is now much lower (Fig. 4), ohmic heating is no longer the major heating term, and energy transfer from the arc dominates. There is a large temperature gradient near the tip of the wire, however, the smooth "knee" in the temperature curve still shows evidence of the earlier ohmic heating. Figure 9B plots the anode temperature profile at $t = 500$ ms, when the system is close to steady state. The "knee" in the temperature profile is sharper at this time as the effect of the earlier ohmic heating has disappeared.

Conclusion

We have developed a model capable of predicting welding arc start-up behavior while collecting experimental data to validate the model and improve our understanding of the phenomena occurring during the process. The comparison of the theoretical predictions and experimental observations for a typical welding arc start-up shows reasonable agreement.

In addition, the predicted results help to elucidate the general features of the welding arc start-up phase. Different phenomena are important during the various phases of start-up, and, under the experimental conditions investigated here, the impact of transient phenomena extended several hundreds of milliseconds after the arc has struck. As described in the previous section, there is an interval when the arc is long and power input is lower than its steady-state value, followed by a short arc phase where the arc current is higher than the steady-state value.

During start-up, instantaneous currents and welding power inputs differ substantially from their final steady values, and this can be expected to result in a deterioration in weld quality (given that the steady-state conditions are well-chosen). A better understanding will help development of improved methods of control during the start-up phase to maintain weld quality, by taking account of the physical phenomena described in the Comparison of Model Predictions with Experiment section. For example, in the case of robotic welding with numerous short welding

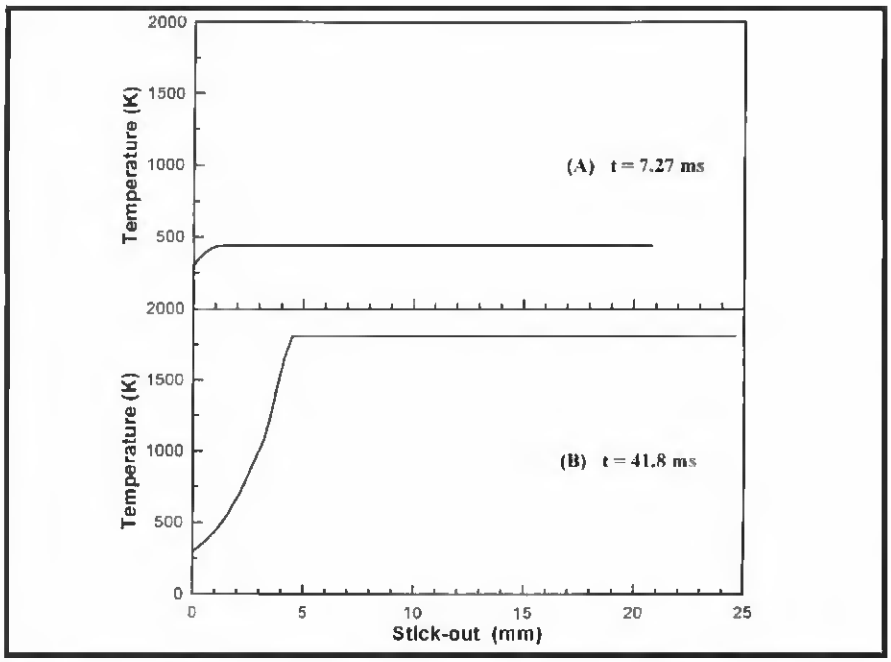

Fig. 8 — The predicted temperature distribution along the anode wire at times A — 7.27 ms, and B — 41.8 ms, just before the anode wire melts. Experimental conditions were the same as in Fig. 4.

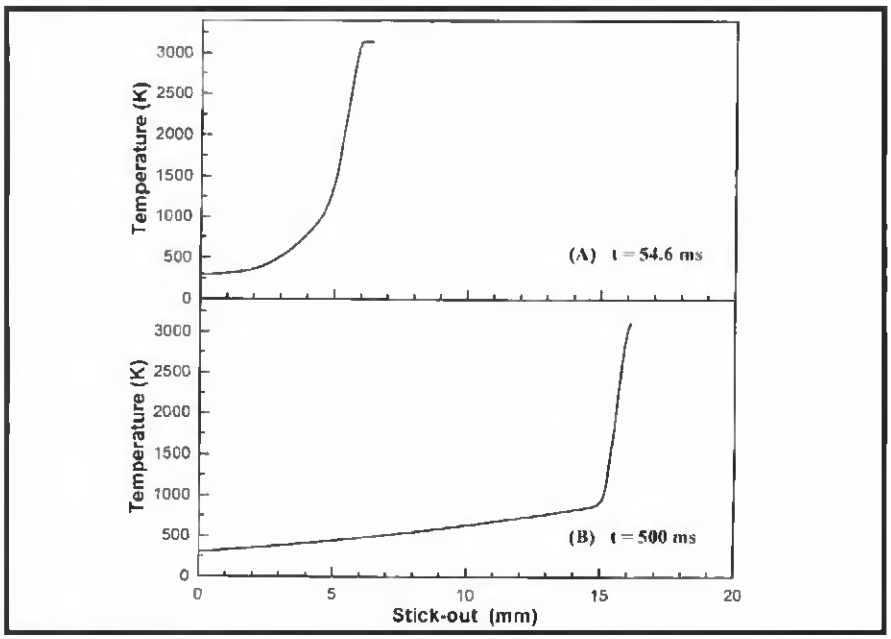

Fig. 9 — The predicted temperature distribution along the anode wire at times A — 54.6 ms, just after the arc has formed, and B — 500 ms. Experimental conditions were the same as in Fig. 4.

runs, control of the start-up phase would be particularly valuable.

Acknowledgments

The authors acknowledge research funding from the Cooperative Research Centre for Materials Welding and Joining and the Australian Research Council. We are also grateful to the ComWeld Group and the British Oxygen Corporation for providing support and assistance. Finally, we thank the CSIRO Division of Applied Physics for the use of the free-burning arc model.

References

1. Lancaster, J. F. 1987. The physics of fusion welding Part I: The electric arc in welding. *IEE Proceedings* 134 Part B: 233–354.

2. Lancaster, J. F. 1987. The physics of fusion welding Part 2: Mass transfer and heat flow. *IEE Proceedings* 134 Part B: 297–316.

3. Waszink, J. H. 1979. Measurements and calculations of the resistance of the wire extension in arc welding. *Proc. Int. Conf. on Arc Physics and Weld Pool Behavior*, The Welding Institute, pp. 227–239.

4. Waszink, J. H., and Van den Heuvel, G. J. P. M.1982. Heat generation and heat flow in the filler metal in GMA welding. *Welding Journal* 61 (8): 269-s to 282-s.

5. Waszink, J. H., and Piena, M. J. 1985. Thermal processes in covered electrodes. *Welding Journal* 64 (2): 37-s to 49-s.

6. Cooksey, C. J., and Milner, D. R. 1962. Metal transfer in gas shielded arc welding. *Proc. Symposium Physics of the Welding Arc*, The Welding Institute, Cambridge, England, pp. 123–132.

7. Jacobsen, N. 1992. Monopulse investigation of drop detachment inpulsed gas metal arc welding. *J. Phys. D: Appl. Phys.* 25: 783–797.

8. Kim, Y-K, McEligot, D. M., and Eagar, T. W. 1991. Analysis of electrode heat transfer in gas metal arc welding. *Welding Journal* 69 (1): 20-s to 31-s.

9. Simpson, S. W., and Zhu, P. 1995. Formation of molten droplets at a consumable anode in an electric welding arc. *J. Phys. D: Appl. Phys.* 28: 1594–1600.

10. Nemchinsky, V. A. 1994. Size and shape of the liquid droplet at the molten tip of an arc electrode. *J. Phys D: Appl. Phys.* 27: 1433–1442.

11. Zhu, P., Rados, M., and Simpson, S. W. 1995. A theoretical study of a gas metal arc welding system. *Plasma Sources Sci. Technol.* 4: 495–500.

12. Simpson, S. W., Zhu, P., and Rados M. 1994. Simulation and observations of the transfer process in gas metal arc welding. *Proceedings of 42nd National Welding Conference*, Vol. 2, Paper 31, Welding Technology Institute of Australia.

13. Lancaster, J. F., ed., 1986. *The Physics of Welding*. p.150, Oxford, Pergamon Press.

14. Lowke, J. J., Kovitya, P., and Schmidt H. P. 1992. Theory of free-burning arc columns including the influence of the cathode. *J. Phys. D: Appl. Phys.* 25: 1600–1606.

15. Law, S. 1995. Laser shadowgraphs in welding diagnostics. *Aust. Optical Soc. News* 9: 17–19.

16. Allemand, C. D., Schoeder R., Ries, D. E., and Eagar, T. W. 1985. A method of filming metal transfer in welding arcs. *Welding Journal* 64 (1): 45–47.